Applied Catalysis B: Environmental 282 (2021) 119511

Contents lists available at ScienceDirect

Applied Catalysis B: Environmental

journal homepage: www.elsevier.com/locate/apcatb

Manipulation of plasmon-induced hot electron transport in Pd/MoO_{3-x}@ZIF-8: Boosting the activity of Pd-catalyzed nitroaromatic hydrogenation under visible-light irradiation

Meicheng Wen[a], Shengnan Song[a], Qiuxia Liu[a], Haibo Yin[b], Kohsuke Mori[b,c,d], Yasutaka Kuwahara[b,c,d], Guiying Li[a], Taicheng An[a,*], Hiromi Yamashit[b,c,*]

[a] Guangdong Key Laboratory of Environmental Catalysis and Health Risk Control, School of Environmental Science and Engineering, Institute of Environmental Health and Pollution Control, Guangdong University of Technology, Guangzhou 510006, China
[b] Graduate School of Engineering, Osaka University, 2-1 Yamada-oka, Suita, Osaka 565-0871 Japan
[c] Unit of Elements Strategy Initiative for Catalysts & Batteries, ESICB, Kyoto University, Japan
[d] JST, PRESTO, 4-1-8 Honcho, Kawaguchi, Saitama 332-0012, Japan

ARTICLE INFO

Keywords:
Plasmonic effect
Schottky junction
Electron flow
Hydrogenation
Nitroaromatics

ABSTRACT

Controlling the charge carrier transfer pathway in a plasmonic catalyst is the key to developing efficient catalyst. Herein, a visible-light responsive plasmonic catalyst is prepared by depositing Pd nanoparticles on ZIF-8 (zeolitic imidazolate framework) coated plasmonic MoO_{3-x} composites (Pd/MoO_{3-x}@ZIF-8). The as-prepared catalyst allows effective plasmon-induced electron transfer from plasmonic MoO_{3-x} to Pd active site by taking advantages of the Schottky junction formed between Pd metal nanoparticles and MoO_{3-x}@ZIF-8 composite as well as heterojunction formed between ZIF-8 and MoO_{3-x}, effectively retarding the recombination of the plasmonic induced hot electron-hole pairs in MoO_{3-x}. As a result, the Pd/MoO_{3-x}@ZIF-8 presents exceptionally higher catalytic activities for the hydrogenation of nitroaromatics under visible-light irradiation than that under dark conditions, which are far superior to those of Pd/MoO_{3-x} and Pd/ZIF-8. The enhanced activity can be attributed to the cooperative promoting effects between Pd nanoparticles and plasmonic MoO_{3-x}@ZIF-8 on facilitating the plasmon-induce electron transfer, and the possible reaction mechanism is proposed. This study expands the scope of reductive organic chemical transformation catalyzed by plasmonic catalysts and sheds light on design of efficient plasmonic catalysts by steering an electron flow to promote the photogenerated electron transfer from plasmonic semiconductor to catalytic active site.

1. Introduction

Hydrogenation of nitroaromatics into the corresponding amines is one of the most important chemical reactions in organic synthesis. Aromatic amines, as valuable intermediate products, have been widely used in the manufacture of fuel additives, pesticides, plastic and rubber industries, drugs and antioxidants [1,2]. In the past decades, many approaches including using different reducing agents, noncatalytic, and catalytic methods, were developed for the reduction of nitroaromatics into amines [3–6]. Among those technologies, catalytic reduction of nitroaromatics into amines has been emerging as a most promising method because of the mild reaction conditions and environmental benign process. Therefore, considerable attention has been paid on the development of efficient catalyst with high catalytic activity and selectivity under mild reaction conditions.

The catalytic hydrogenation of nitro group with hydrogen or hydrogen carriers requires the heterolytic cleavage of H_2 (H^+/H^- pair). Therefore, a large number of Pd, Pt, and Ru nanoparticle supported catalysts have been used in chemoselective hydrogenation of nitroaromatics to amines due to their high affinity to H_2 and considerable achievements have been obtained in recent years [7–9]. However, the catalytic process usually requires high temperature and H_2 pressure, and most of catalysts do not meet the dual requirements of high chemoselectivity and activity due to the weak binding force of nitro group to noble metal active sites and the difficult in the cleave of stable N–O bond. Evidently, designing a suitable catalyst for the hydrogenation of nitroaromatics to the corresponding amines with high chemoselectivity and activity under mild conditions is highly desirable.

In recent years, semiconductor based plasmonic catalysts have been widely used to improve the efficiency of catalysis either by their intense

* Corresponding author.
E-mail addresses: antc99@gdut.edu.cn (T. An), yamashita@mat.eng.osaka-u.ac.jp (H. Yamashit).

https://doi.org/10.1016/j.apcatb.2020.119511
Received 26 December 2019; Received in revised form 28 August 2020; Accepted 30 August 2020
Available online 06 September 2020

visible/near-infrared response or efficient charge separation. A large amount of free charge carriers in plasmonic catalysts oscillate with incident light, leading to the localized surface plasmon resonances (LSPRs) [10,11]. As a result, hot electrons with high energy are generated through LSPR effect, and subsequently can be involved in redox reaction [12,13]. Our very recent works have successfully demonstrated that plasmonic hot electrons are very unique for improving the catalytic activity and selectivity in hydrogenation of nitroaromatics [14]. The plasmon-induced hot electrons migrate from plasmonic catalyst to metal nanoparticles through Schottky junction, which greatly change the electron density of metal nanoparticle [15,16], and then result in the formation of charged catalytic active site for enhancing the binding force of nitro group to metal surface and promoting the dissociation of N–O bond [14]. Nevertheless, a fast recombination rate of plasmon-induced charge carries still hinders the commercial application of plasmonic catalyst as the catalytic activity highly depends on the separation and transfer of charge carriers [17]. Apart from the Schottky junction, recent progress has demonstrated that the separation and transfer of plasmon-induced charge carriers can also be potentially enhanced by integrating plasmonic catalysts with other semiconductor by forming heterojunction between plasmonic catalyst and semiconductor with high electron migration [18–20]. Increasing efforts have been made to achieve metal organic framework (MOF) loaded with semiconductor/plasmonic materials photocatalysts for various photocatalytic reaction including hydrogen evolution from hydrogen carriers, organic compounds transformation as well as environmental purification [21–26]. The use of MOF has been demonstrated as an effective strategy for promoting the photogenerated charges separation due to their semiconducting property, high surface area and porosity, unique atomic/molecular coordination as well as tunable bandgap [27,28]. There is no doubt about the functions of Schottky barrier formed between metal nanoparticle and MOFs as well as heterojunction formed between MOFs and plasmonic catalyst in maneuvering the migration rate of plasmon-induced hot electrons. However, the rational arrangement of Schottky junction and heterojunction to steer an electron flow for fast and continuous hot electron injection is still one of great challenge.

Herein, on the basis of above discussion, a novel plasmonic catalyst Pd/MoO_{3-x}@ZIF-8 is prepared by coating ZIF-8 (zeolitic imidazolate frameworks) on the surface of plasmonic MoO_{3-x} catalyst and by decorating Pd nanoparticles on the surface of ZIF-8. MoO_{3-x}, as non-noble metal based plasmonic catalyst, displays strong LSPR in the visible light region. The heterojunction formed between plasmonic MoO_{3-x} and ZIF-8 is to inject plasmon-induced electrons into the LUMO of ZIF-8. On the other hand, the Pd loaded on the surface of ZIF-8 is to establish a Schottky junction as the charge “pump”, which steers the migration of electron from the LUMO of ZIF-8 to the Pd active site, thus greatly accelerating plasmon-induced electron transfer from MoO_{3-x} to Pd active sites. As expected, Pd/MoO_{3-x}@ZIF-8 presents exceptionally higher catalytic activities for the hydrogenation of nitroaromatics under visible-light irradiation than that under dark conditions, and are far superior to those of Pd/MoO_{3-x} and Pd/ZIF-8. The photocurrent measurement further confirmed the fast separation and transfer of plasmon-induced charge carriers within Pd/MoO_{3-x}@ZIF-8.

2. Experimental

2.1. Preparation of catalysts

The PVP modified plasmonic MoO_{3-x} is prepared according to our published paper [13]. In a typical procedure, molybdenum metal powder (2 mmol) was dispersed into ethanol (24 mL) under magnetically stirring, then followed by adding H_2O_2 (3 mL, 30 wt%) to obtain a yellow solution, then the solution was transferred into a Teflon vessel and sealed in stainless steel autoclave, heated and maintained at 160 °C for 12 h. After cooling to room temperature, the product was washed with ethanol and water three times respectively and dried under vacuum for overnight. PVP modified MoO_{3-x} was prepared by dispersion of MoO_{3-x} (100 mg) in methanol containing 240 mg PVP under magnetically stirring for 30 min, then the product was separated by centrifugation and washed with methanol for six times and dried under vacuum for overnight.

MoO_{3-x}@ZIF-8 composite was prepared by in-situ growth method. Typically, solution A was prepared by dissolving 2-methylimidazole (0.5 mmol) into methanol (20 mL), and solution B was prepared by dissolving zinc nitrate hexahydrate (0.5 mmol) into methanol (20 mL), then MoO_{3-x} (15 mg, modified with PVP) was dispersed into solution A under ultrasonicated for 5 min, solution B was added to the above solution, and keep the mixture at water bath (30 °C) for overnight. Finally, the product was washed with methanol and water three times respectively and dried under vacuum condition overnight. Furthermore, MoO_{3-x}@ZIF-8−5 with thick shell was adopted by different recipe, in which 5 mg MoO_{3-x} is added into solution A, then, followed by similar procedure.

Pd loaded catalysts were prepared by following steps: Palladium acetate (0.075 mmol) was dissolved in methanol (150 mL) at water bath (30 °C) under magnetically stirring. After 15 min stirring, MoO_{3-x}@ZIF-8 (0.15 g) was dispersed into above solution, and continuously stirred for 30 min, then the product was separated by centrifugation and washed with ethanol for six times noted as Pd/MoO_{3-x}@ZIF-8. References sample, Pd/MoO_{3-x}@ZIF-8−0 and Pd/MoO_{3-x}@ZIF-8−9 was also prepared without washing and with nine times of ethanol washing, respectively. Pd/ZIF-8 and Pd/MoO_{3-x} was synthesized with similar procedure. Finally, all products were dried under vacuum for overnight. All samples are stored in the vacuum condition at room temperature with the aim to prevent the oxidation of sample by air. The loading amount of Pd was determined by ICP to be 3.2 wt %, 3.1 %, and 3.2 % for Pd/MoO_{3-x}@ZIF-8, Pd/ZIF-8, and Pd/MoO_{3-x}, respectively. Furthermore, the weight amount of Zn and Mo was also measured by ICP to be 5.95 % and 22.9 % for Pd/MoO_{3-x}@ZIF-8, respectively.

2.2. Catalysts characterization

Nitrogen sorption analysis was performed on a BEL-SORP max system (BEL Japan, Inc.) at 77K. Samples were degassed at 150 °C for 24 h prior to analysis. XRD pattern was performed on a RigakuRINT2500 Ultima IV X-ray diffractometer with Cu Kα radiation (λ = 1.5406 Å). The electronic state of Mo element was recorded using a Shimadzu ESCA 3200 photoelectron spectrometer with Mg Kα radiation, and C 1s (284.6 eV) was used to calibrate the binding energies of the elements. UV–vis diffuse reflectance spectra of samples were investigated using a Shimadzu UV-2450 spectrophotometer with BaSO4 as the standard reference. Pd K-edge XAFS measurements were carried out at the beamline BL01B1 station in fluorescence mode with an attached Si (111) monochromator at SPring-8, Harima, Japan (prop. No. 2014 A1045). Time-resolved fluorescence spectroscopy was recorded on an Edinburgh FLS920 spectrophotometer. Field emission-transmission electron microscope (FE-TEM, Hitachi Hf-2000f, Japan) equipped with energy dispersive X-ray spectroscopy was used to analyze the morphologies and elemental maps of samples.

2.3. Activity test

60 mM solution of nitrobenzene and 60 mM solution of ammonia borane (AB) in ethanol were separately prepared. 10 mg of catalyst was weighed and dispersed in the sealed reactor tube. 5 mL of nitrobenzene solution was injected through the rubber septum followed by Ar bubbling for 15 min to ensure the inert atmosphere conditions. Reaction was initiated upon addition of 5 mL of AB solution through the rubber septum in the reactor tube. The catalytic reaction was conducted under continuously stirring in dark or under visible light irradiation (Xe lamp (300 W) equipped a UV cutoff filter (> 420 nm)) conditions at 30 °C for

1 h. The products were analyzed by using Shimadzu GC-2010 chromatograph.

2.4. Electrochemical measurements

Photoelectrochemical properties were tested on a CHI 600E electrochemical workstation (Chenhua Instrument, China) with a typical three-electrode system. The Pt foil and Ag/AgCl serve as the counter and reference electrodes, respectively. 0.5 M Na_2SO_4 aqueous solution was utilized as electrolyte and a Xe lamp (300 W) equipped a UV cutoff filter (> 420 nm) was employed as visible light source. For the preparation of working electrode, a suspension was prepared by adding 2 mg of catalyst and 30 μL of Nafion into 2 mL of ethanol, and ultrasonicated for 15 min. Then, 50 μL of suspension was drop-casted onto an indium-tin oxide (ITO) glass substrate and further dried to remove the organic residuals.

3. Results and discussion

3.1. Catalyst characterization

PVP modified plasmonic MoO_{3-x} nanosheet, possessing strong LSPR in the visible light region, was employed as the core of Pd/MoO_{3-x}@ZIF-8. To build heterojunction, ZIF-8 was coated on the surface of MoO_{3-x} nanosheet through in-situ growth method, and the Schottky junction was constructed by deposing Pd nanoparticles (electron acceptors) on the surface of ZIF-8 through mild reduction method in the presence of methanol as a reductant and PVP as a stabilizer (details in the Supporting Information). X-ray diffraction (XRD) was used to characterize the phase structure of as-prepared samples. As shown in Figure S1, the X-ray diffraction pattern of MoO_{3-x} is assigned to the orthorhombic phase (JCPDS No. 5-508). Meanwhile, the peaks of pure ZIF-8 are consistent with the previous reports [29], and the presence of strong peaks indicates high crystallinity of the prepared ZIF-8. For MoO_{3-x}@ZIF-8, the intensities of diffraction peaks decreased as compared with the virgin ZIF-8. This behavior is likely due to the deposition of ZIF-8 on the surface of MoO_{3-x} causing peaks interference. Evidently, the XRD results suggested that ZIF-8 was successfully deposited on the MoO_{3-x}. Figure S2 shows BET (Brunauer–Emmett–Teller) surface areas of all samples tested by N_2 adsorption isotherm measurements. Sample ZIF-8 and MoO_{3-x}@ZIF-8 display Type-I behavior with completely reversible isotherm, demonstrating the microporous structure of samples. Meanwhile, MoO_{3-x} exhibited Type-III behavior with nonporous structure. The surface areas of ZIF-8, MoO_{3-x}@ZIF-8, and MoO_{3-x} were determined to be 1110 $m^2 g^{-1}$, 521 $m^2 g^{-1}$, and 14.6 $m^2 g^{-1}$, respectively. These results clearly indicate that the surface area of MoO_{3-x}@ZIF-8 is higher than that of MoO_{3-x}. However, the N_2 uptake is decreased as compared with ZIF-8 and no hysteresis loop is observed for MoO_{3-x}@ZIF-8, suggesting a decrease in the number of micropores and no mesopore structure was formed as compared with ZIF-8.

Transmission electron microscopy (TEM) offers direct information on morphology and structure of Pd/MoO_{3-x}@ZIF-8 with high spatial resolution. Fig. 1a reveals that MoO_{3-x} with nanosheet structure (Figure S3a) is surrounded by ZIF-8 particles, suggesting the successful growth of ZIF-8 particles on the surface of MoO_{3-x}. In this study, PVP severs as surfactant playing a key role in inducing the nucleation of ZIF-8 on the surface of MoO_{3-x}, leading to the formation of MoO_{3-x}@ZIF-8 with core-shell structure. In contrast, no core-shell structure can be observed in the absence of PVP as surfactant (Figure S3b). In order to verify the reproducibility of this synthetic experiment. The synthetic experiment is run in triplicate, it can be clearly observed that MoO_{3-x}@ZIF-8 with core-shell structure and similar thickness can be clearly observed in the repeated experiment as shown in Figure S3c and Figure S3d, suggesting the good reproducibility of the synthesis. The average thickness of the shell is measured to be around 144 nm. Figure S4 presents the TEM images of different samples, Pd nanoparticle with average particle size of 1.9, 1.8 and 4.5 nm was observed for Pd/MoO_{3-x}@ZIF-8, Pd/ZIF-8 and Pd/MoO_{3-x}, respectively. HAADF-STEM image of Pd/MoO_{3-x}@ZIF-8 (Fig. 1b) further demonstrated the well-defined core-shell structure of Pd/MoO_{3-x}@ZIF-8. Meanwhile, elemental mapping indicates separable distribution of the characteristic elements, including Mo, N, Zn, and Pd, are all present and homogeneously distributed throughout the materials area as shown in Fig. 1c-f. it is clearly indicates that the Mo is mainly distributed in the core part of Pd/MoO_{3-x}@ZIF-8 structure, indicating MoO_{3-x} is in the core part. On the other hand, the density of N, and Zn on the shell part is higher than that of core part, further confirming the successful growth of ZIF-8 particles on the surface of MoO_{3-x}. It was found that Pd element is uniformly distributed on the shell part of Pd/MoO_{3-x}@ZIF-8 structure, further verifying the core-shell structure of Pd/MoO_{3-x}@ZIF-8.

X-ray photoelectron spectroscopy was used to elucidate the chemical state of Mo. Fig. 2a displayed the fitted Mo 3d core level spectra of Pd/MoO_{3-x} and Pd/MoO_{3-x}@ZIF-8. Binding energy peaks of Pd/MoO_{3-x} and Pd/MoO_{3-x}@ZIF-8 at 232.4 and 235.8 eV can be assigned to $3d_{5/2}$ and $3d_{3/2}$ of Mo^{6+} species at higher oxidation state, and the peaks of Pd/MoO_{3-x} and Pd/MoO_{3-x}@ZIF-8 located at 231.4 and 234.6 eV are assigned to Mo^{5+}. In addition to Mo^{6+} and Mo^{5+} ions observed in Pd/MoO_{3-x}@ZIF-8, Mo^{4+} (binding energy at 229.7 and 233.2 eV) with lower oxidation state are also observed in Pd/MoO_{3-x}@ZIF-8, which is probably due to the mild reducibility of methanol during the ZIF-8 growth and Pd reduction. Given that the peak area of Mo^{6+}, Mo^{5+}, and Mo^{4+} ions was determined to be 43.3 %, 43.4 % and 13.3 %, respectively [13], the average oxidation state of Mo in Pd/MoO_{3-x}@ZIF-8 is calculated to be 5.30, demonstrating the abundant oxygen vacancies in Pd/MoO_{3-x}@ZIF-8. Furthermore, the oxidation state of Pd species on Pd/MoO_{3-x} and Pd/MoO_{3-x}@ZIF-8 was also investigated by X-ray absorption fine structure (XAFS) measurements. Fig. 2b shows the Fourier transforms (FTs) of k^3-weighted Pd K-edge extended X-ray absorption fine structure (EXAFS) of different samples. The reference sample Pd foil exhibited an intensive doublet peak located at 2.6 Å, which is ascribed to a single metallic bond (Pd-Pd), and the reference sample Pd $(OAc)_2$ displays an intensive single peak at 1.6 Å which is assignable to Pd-O bond. Similar to that of Pd foil, the spectrum of Pd/MoO_{3-x} and Pd/MoO_{3-x}@ZIF-8 both exhibited an intense peak located at 2.6 Å, which is corresponded to Pd–Pd bond in a metallic form, clearly suggesting that the Pd species on MoO_{3-x} and MoO_{3-x}@ZIF-8 is in a metallic form [30].

Fig. 3 displays the optical response of samples Pd/MoO_{3-x}, Pd/MoO_{3-x}@ZIF-8, and Pd/ZIF-8 investigated by UV–vis spectrometer. Pd/ZIF-8 exhibited an adsorption band in the high energy region (λ < 300 nm) and showed complete transparency to light absorption with wavelength longer than 300 nm. In contrast, a strong absorption peak located at approximately 900 nm associated with LSPR is clearly observed in the spectra of Pd/MoO_{3-x}. As well known that the optical property of plasmonic materials is very sensitive to the surrounding environment. After the deposition of ZIF-8 on MoO_{3-x} nanosheets, the light adsorption intensity of Pd/MoO_{3-x}@ZIF-8 in the low energy region (λ > 400 nm) showed apparent decrease accompanied with the blue shift of the adsorption edge in the high energy region (λ < 400 nm) compared with that of Pd/MoO_{3-x}. Possible explanation is that the ZIF-8 shell prevents the visible light irradiation on plasmonic MoO_{3-x}, leading to the low absorption efficiency at low energy region (λ > 400 nm). The results demonstrate that Pd/MoO_{3-x}@ZIF-8 is a visible-light-absorbing catalyst showing a great potential in the conversion of visible light for promoting Pd-catalyzed hydrogenation of nitroaromatics.

3.2. Catalytic test

The catalytic activity of Pd/MoO_{3-x}@ZIF-8 was examined by nitrobenzene reduction. The catalytic reaction was conducted in the sealed reactor containing ammonia borane (NH_3BH_3) as a H_2 source both under visible light irradiation and in the dark. No product was

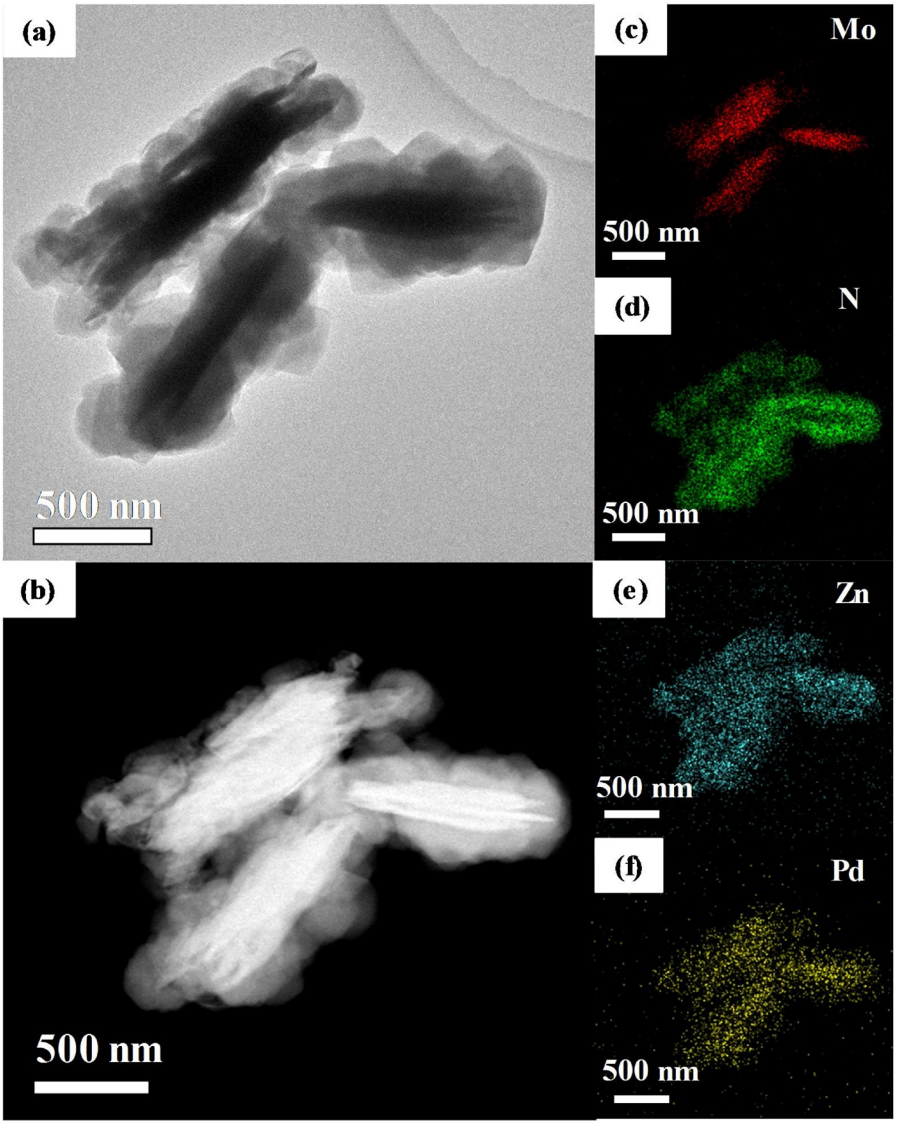

Fig. 1. (a) TEM and (b) HAADF-STEM image of Pd/MoO_{3-x}@ZIF-8, and (c-f) EDX spectra of (c) Mo, (d) N, (e) Zn, and (f) Pd element, respectively.

detected over MoO_{3-x}@ZIF-8, ZIF-8, and MoO_{3-x}, demonstrating that Pd nanoparticles is necessary for catalyzing this reaction. As shown in Fig. 4, all samples Pd/MoO_{3-x}@ZIF-8, Pd/ZIF-8, and Pd/MoO_{3-x} display similar activity in the dark conditions, affording 53 %, 50 %, 45 % yields, respectively. Negligible enhancement occurred over Pd/ZIF-8 even under visible light irradiation. In contrast, a considerable enhancement of activity was obtained over Pd/MoO_{3-x} under visible light irradiation, which might be attributed to the plasmonic effect of MoO_{3-x} in generating hot electrons and the formation of activated Pd species after the absorption of incident visible light. It is noteworthy that a further significant enhancement of activity was achieved on Pd/MoO_{3-x}@ZIF-8 under visible light irradiation, 42 % higher than that of under dark condition and 27 % higher than that of Pd/MoO_{3-x} under the same reaction conditions. The enhanced catalytic activity might be attributed to the cooperative effect between MoO_{3-x}@ZIF-8 with core-shell structure and Pd nanoparticles in steering electron flow transferred from MoO_{3-x} to Pd nanoparticles, resulting in fast separation and transfer of plasmon-induced electron, leading to the enhancement of intrinsic catalytic activity of Pd-catalyzed nitrobenzene reduction. As a proof of concept demonstration, Pd/MoO_{3-x}/ZIF-8 was prepared by physically mixing 5 mg MoO_{3-x} with 10 mg Pd/ZIF-8 as a reference sample and was examined in the reaction. As shown in Figure 4, 49 % yield was obtained over Pd/MoO_{3-x}/ZIF-8 in the dark conditions, and slightly improved activity was observed under visible light irradiation, probably due to the occasional hot electron transfer from MoO_{3-x} to Pd nanoparticles. In addition, the influence of the shell thickness on catalytic performance is studied. Pd/MoO_{3-x}@ZIF-8 with thick ZIF-8 shell was adopted by different recipe. it can be seen from Figure S3e that the thickness of Pd/MoO_{3-x}@ZIF-8 shell was increased with decreasing the amount of MoO_{3-x}. The catalytic performance of Pd/MoO_{3-x}@ZIF-8 samples with different shell thickness was shown in Figure S5, all samples displayed similar catalytic activities under dark conditions. Upon visible light irradiation, the catalytic activity of Pd/MoO_{3-x}@ZIF-8 with average shell thickness of 144 nm is slightly higher than that of MoO_{3-x}@ZIF-8 − 5 with average shell thickness of 251 nm, demonstrating that the shell thickness slightly affects the electron transfer. It can be observed from Fig. 1a and Figure S3e that the shell of composites is constructed by ZIF-8 nanoparticles. It is clear that Pd nanoparticles not only existed on the external surface of composites, but also exited on the internal surface of composites. Therefore, it is easy to understand that the shell thickness didn't display significant impact on catalytic performance. These observations demonstrate the cooperative effect between MoO_{3-x}@ZIF-8 with core-shell structure and Pd nanoparticles in steering electron flow transferred from MoO_{3-x} to Pd nanoparticles.

It is well known that PVP is widely used as surfactant to synthesized Pd nanoparticles with small size. In this study, it is difficult to

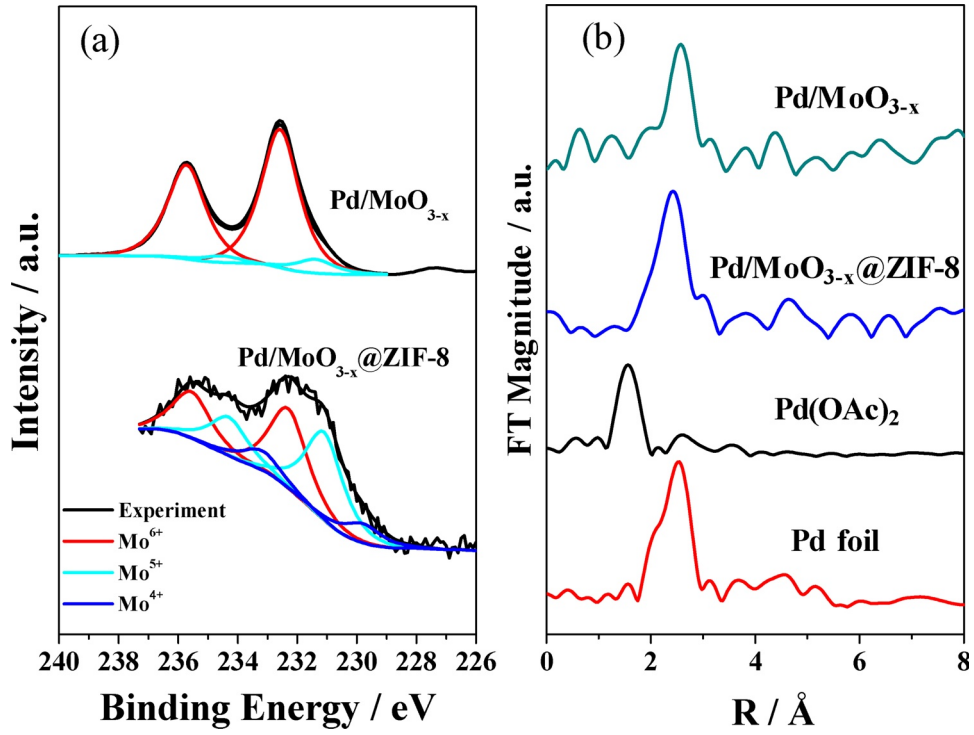

Fig. 2. (a) Mo 3d XPS spectra of the Pd/MoO_{3-x} and Pd/MoO_{3-x}@ZIF-8. (b) Pd K-edge FT-EXAFS spectra for Pd foil, $Pd(OAc)_2$, Pd/MoO_{3-x}, and Pd/ MoO_{3-x}@ZIF-8.

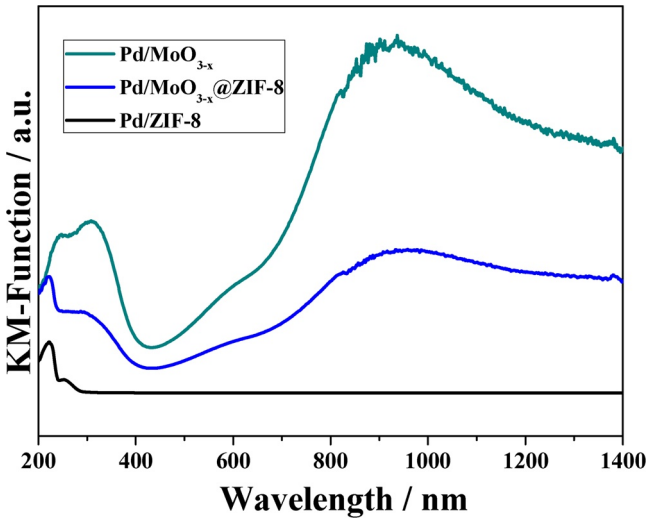

Fig. 3. UV − vis − NIR spectra of samples Pd/MoO_{3-x}, Pd/MoO_{3-x}@ZIF-8, and Pd/ZIF-8 and wavelength dependence of the enhancement of catalytic performance of Pd/MoO_{3-x}@ZIF-8 under irradiation by monochromatic light (λ = 400 nm, 6 mW cm^{-2}, an LED lamp (λ = 530 nm, 10 mW cm − 2).

completely remove PVP from the as-synthesized Pd nanoparticles. Hence, it is important to investigate the effect of PVP on the Pd surface because they interact with the active sites and can alter the electronic structure of Pd. In order to investigate the effect of PVP on catalytic activity, the catalytic reactions were performed over Pd/MoO_{3-x}@ZIF-8 − 0 without ethanol washing, Pd/MoO_{3-x}@ZIF-8 with six times of ethanol washing, and Pd/MoO_{3-x}@ZIF-8 − 9 with nine times of ethanol washing, respectively. As shown in Figure S6, the highest catalytic activity increased with the increase of washing times, However, similar catalytic activities were observed over Pd/MoO_{3-x}@ZIF-8 and Pd/ MoO_{3-x}@ZIF-8 − 9. For comparison, additional catalytic reaction were performed over Pd/MoO_{3-x}@ZIF-8 by adding 5 mg of PVP in catalytic reaction, and the catalytic activity decreased after adding PVP, demonstrating the negative effect of PVP on catalytic reaction due to the strong interaction between Pd and PVP in changing the electron density of Pd and preventing the adsorption of substrate during the catalytic process.

The light emitted from Xe lamp at λ > 420 nm contains not only visible light but also a part of infrared light. In fact, the temperature of the suspension of Pd/MoO_{3-x}@ZIF-8 slightly heated up (measured to be around 33 °C) under light irradiation. In order to elucidate the effect of infrared thermal heating derived from Xe lamp. Several reactions were carried out at 30, 35, 40, 45, and 60 °C without light irradiation. As shown in Figure S7, the highest catalytic activity was achieved under visible light irradiation at 30 °C, followed by thermal heating at 60, 45, 40, 35 and 30 °C under dark conditions. Furthermore, wavelength-dependent catalytic reactions were also performed under different monowavelength irradiation by using Xe lamp equipped with different band-pass filters (475, 550, and 650 nm) and LED lamp irradiation (980 nm), the intensities of the irradiated light were tested to be 20 mW cm^{-2}. As presented in Figure S8, the increasing yields of catalytic performance with light intensities were well consistent with the light absorption of Pd/MoO_{3-x}@ZIF-8. The largest enhancement of 1.15 % $(mW\ cm^{-2})^{-1}$ was found with the wavelength of λ = 980 nm, which can be assigned to plasmonic effect. Moreover, the reaction yield over Pd/MoO_{3-x}@ZIF-8 under light irradiation with the wavelength of λ = 980 nm was almost linearly dependent on the light intensity (Figure S9), which provides direct evidence that the improved catalytic activity is due to the light irradiation. These results clearly demonstrated that the enhanced activity for Pd-catalyzed hydrogenation of nitroaromatics into corresponding amines is essentially caused by plasmonic effect of MoO_{3-x} in converting visible light to chemical energy, and efficient hot-electron migration in Pd/MoO_{3-x}@ZIF-8.

3.3. Photoelectrochemical tests and Time-resolved transient PL decay spectroscopy

The photoelectrochemical tests was studied and offers important hints for plasmon-induced hot electron transfer and recombination. As shown in Fig. 5a, Pd/ZIF-8 exhibit negligible photocurrent responses under intermittent illumination, suggesting that no electron transfer occurred in Pd/ZIF-8 because Pd/ZIF-8 is inactive under visible light

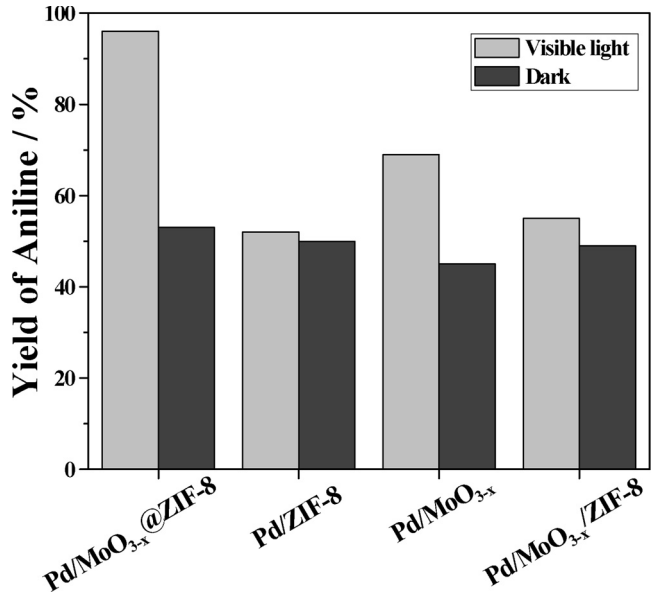

Fig. 4. The comparison of nitrobenzene reduction activity in 60 min with NH_3BH_3 as a reducing agent over different samples at 30 °C, both under visible light irradiation and in the dark.

irradiation as evidenced in Fig. 3, and this is also well consistent with the catalytic performance of Pd/ZIF-8. In contrast, Pd/MoO_{3-x}, Pd/MoO_{3-x}/ZIF-8, and Pd/MoO_{3-x}@ZIF-8 exhibit rapid photocurrent responses under intermittent illumination, which are stable and can be well repeated in several on-off cycles. It can be observed that Pd/MoO_{3-x} displayed a considerable high photocurrent intensity due to the hot-electrons derived from visible light irradiation on plasmonic MoO_{3-x} and transferred from plasmonic MoO_{3-x} to Pd through Schottky junction. Moreover, the photocurrent intensity was greatly improved within Pd/MoO_{3-x}@ZIF-8, elucidating that the heterojunction formed between ZIF-8 and MoO_{3-x} as well as Schottky junction formed between ZIF-8 and Pd steers the plasmonic-induced hot electron migration from MoO_{3-x} to Pd nanoparticles, further effectively retarding the recombination of the plasmonic induced hot electron-hole pairs in MoO_{3-x}. However, the photocurrent intensity decreased within Pd/MoO_{3-x}/ZIF-8, which could be attributed to the ineffective interfacial charge transfer from MoO_{3-x} to Pd nanoparticles. The improved charge carrier separation efficiency is also confirmed by the time-resolved transient PL decay spectroscopy. Obviously, the Pd/MoO_{3-x}@ZIF-8 displayed a slower exponential decay as shown in Fig. 5b. The calculated average lifetime of the Pd/MoO_{3-x}@ZIF-8 (2.51 ns) is distinctly prolonged in comparison with that of Pd/MoO_{3-x} (1.57 ns) and Pd//MoO_{3-x}/ZIF-8 (1.42 ns). The observed long carrier lifetime suggests that the novel structure of Pd/MoO_{3-x}@ZIF-8 greatly enhanced the charge separation, which are beneficial to boosting Pd-catalyzed hydrogenation of nitrobenzene derivatives.

3.3. Possible reaction mechanism

On the basis of above discussion, the possible reaction mechanism for the hydrogenation of nitrobenzene derivatives over plasmonic Pd/MoO_{3-x}@ZIF-8 under visible light irradiation is proposed and depicted in Fig. 6. In the case of MoO_{3-x}, abundant oxygen vacancies make free carries on conduction band of MoO_{3-x}, which occur in oscillation with visible light to exhibit plasmon effect, Initially, the hot-electron with high energy was excited to be hot electron on high energy level through plasmonic effect under visible light irradiation. Then, the plasmonic induced energetic hot-electrons are not only transfer to the LUMO state of ZIF-8 through heterojunction formed between MoO_{3-x} core and ZIF-8 shell but also directly injected into Pd nanoparticle. This possible charge transfer pathway can also be demonstrated by recent studies. [12,18,29,30] On the other hand, the hot electrons are further migrated and trapped by Pd nanoparticle, leading to the formation of electron rich-Pd nanoparticles. Generally, the catalytic process of nitroaromatic hydrogenation over Pd nanoparticle usually involves adsorption of nitroaromatic onto metallic Pd nanoparticle to form an activated complex species, followed by the dissociation of stable N–O bond and the formation of N−H bond in the presence of H_2 source. However, the weak binding force of nitro group to noble metal active sites and the difficulty in the cleave of stable N–O bond hinder the catalytic activity of Pd-based catalyst. In this study, the intrinsic catalytic activity of Pd-catalyzed hydrogenation of nitrobenzene derivatives was promoted owing to high-density electron of Pd nanoparticle, in which the nitro group of nitroaromatic could be efficiently captured and activated, and the H_2 generated by the dehydrogenation of NH_3BH_3 was also promoted as evidenced by our previous results. [11,14] Meanwhile, the plasmonic induced positive charge probably reacts with H_2O to form hydroxyl radical (˙OH), then followed by reacting with NH_3BH_3 to produce H_2 [31]. Finally, the consumed electrons during the reaction is constantly replenished by the dehydrogenation of NH_3BH_3. Overall, the hot electron charge flow steered in Pd/MoO_{3-x}@ZIF-8 is mainly attributed to the rationally catalyst design and architecture, triggering the plasmonic electron injection from MoO_{3-x} to ZIF-8 as well as Schottky barrier electron trapping from ZIF-8 to Pd species.

With the understanding of the reaction mechanism, the catalytic activity of Pd/MoO_{3-x}@ZIF-8 was further estimated by using various nitrobenzene derivatives as the starting materials and the results are listed in Table 1. The typical catalyst Pd/MoO_{3-x}@ZIF-8 exhibited a higher catalytic activity for a series of substituted nitroaromatic compounds than that in the dark conditions. Among them, 4-nitrophenol, 3-nitrophenol, p-nitroaniline, and 4-nitrotoluene gave the complete conversion and selectivity without generating by-product (entry 2, 3, 4 and

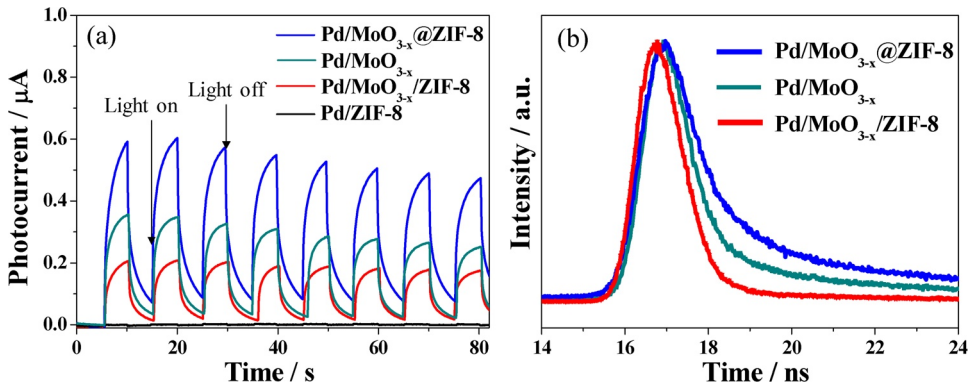

Fig. 5. (a) Photocurrent responses of different samples with or without visible light irradiation, (b) time-resolved transient PL decay curves of different samples under the excitation wavelength of 450 nm.

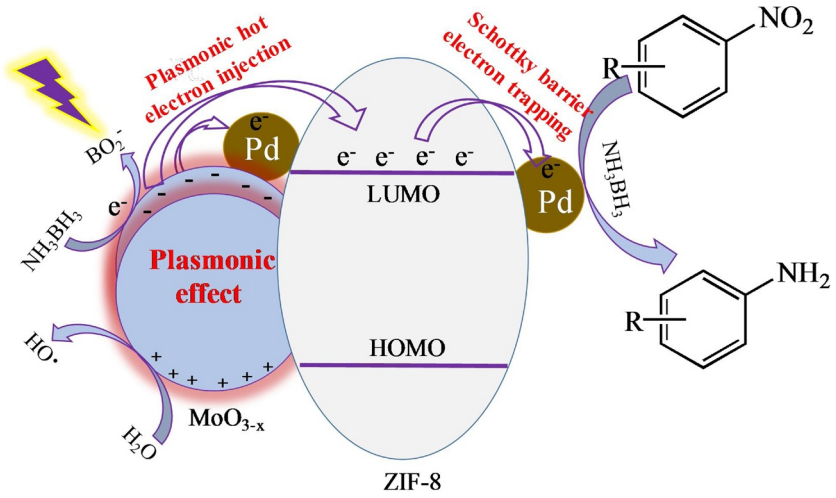

Fig. 6. Schematic illustration of possible reaction mechanism for the hydrogenation of nitrobenzene derivatives over plasmonic Pd/MoO_{3-x}@ZIF-8.

Table 1
Hydrogenation of substituted nitrobenzene over Pd/MoO_{3-x}@ZIF-8 with NH_3BH_3 as reducing agent.

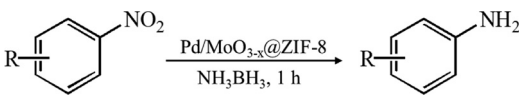

Entry	R	Product	Yields [a]	Yields [b]
1	-H	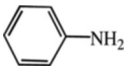	96 %	53 %
2	-OH	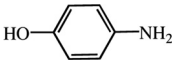	100 %	76 %
3	-OH	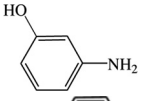	99 %	73 %
4	-NH_2		99 %	69 %
5	-CH_3	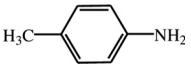	95 %	65 %
6	-CH = CH_2	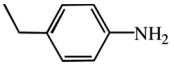	98 %	70 %
7	-Cl	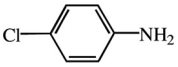	70 %	30 %
8	-Cl	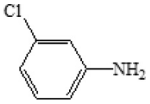	67 %	29 %
9	-Br	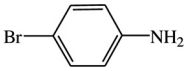	76 %	40 %
10	-COOH	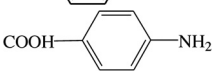	78 %	35 %
11[c]	-H	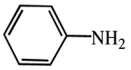	37 %	47 %

[a] Reaction conditions: 10 mg catalyst, 0.3 mmol substrate, 0.3 mmol NH_3BH_3, 10 mL ethanol, reaction time: 1 h, reaction temperature: 30 °C, under visible light irradiation.
[b] Reaction carried out in the dark conditions.
[c] NH_3BH_3 was replaced by 1 bar hydrogen.

5). In case of 4-nitrostyrene bearing olefinic bonds, can also be fully converted into 4-ethylaniline (98 % yield) under visible light irradiation (entry 6). 4-chloronitrobenzene, 3-chloronitrobenzene, 1-bromo-4-nitrobenzene, and 4-nitrobenzoic acid also displayed a considerable yield in the reaction system (entry 7, 8, 9 and 10). With the rational design and architecture of plasmonic Pd/MoO_{3-x}@ZIF-8, the attractive catalytic activity in the hydrogenation of a series of nitro compounds bearing diverse groups under mild conditions was realized by converting visible light to chemical energy with the help of plasmonic Pd/MoO_{3-x}@ZIF-8. The stability test of Pd/MoO_{3-x}@ZIF-8 was also evaluated by the hydrogenation of nitrobenzene. As shown in Figure S10, the catalytic activity of Pd/MoO_{3-x}@ZIF-8 showed no significant change even after reuse for six times, demonstrating the high stability of plasmonic Pd/MoO_{3-x}@ZIF-8. Moreover, the morphology and Pd nanoparticle size of recycled sample was investigated by TEM (Figure S11), the core-shell structure was maintained (Figure S11a) after recycling test. However, Pd aggregates was observed (Figure S11b) after recycling test.

4. Conclusions

In summary, we described a facile strategy for the integration of plasmonic MoO_{3-x} nanosheet within porous ZIF-8, which allows highly effective light energy absorption to be used for promoting the intrinsic catalytic activity of Pd-catalyzed nitrobenzene reduction. The designed Pd/MoO_{3-x}@ZIF-8 exhibited the highest catalytic activity under visible light irradiation, which was far superior to those of Pd/MoO_{3-x} and Pd/ZIF-8. The electron-rich Pd nanoparticles generated by charge separation derived from plasmonic effect of MoO_{3-x} plays critical roles in enhancing the catalytic activity. The photocurrent responses experiment results demonstrated that both the heterojunction and Schottky barrier are critical factors to the plasmon-induced hot-electron separation and charge accumulation at surface of Pd nanoparticles. It is anticipated that this work casts new light on the utilization of a variety of plasmonic materials for visible-light enhanced metal-catalyzed chemical reactions.

CRediT authorship contribution statement

Meicheng Wen: Conceptualization, Methodology, Investigation, Writing - original draft, Funding acquisition. **Shengnan Song:** Conceptualization, Methodology, Investigation, Validation. **Qiuxia Liu:** Conceptualization, Methodology, Investigation. **Haibo Yin:** Methodology, Investigation, Validation. **Kohsuke Mori:** Writing - review & editing, Supervision. **Yasutaka Kuwahara:** Writing - review & editing, Supervision. **Guiying Li:** Writing - review & editing, Supervision. **Taicheng An:** Conceptualization, Writing - review &

editing, Supervision, Project administration, Funding acquisition. **Hiromi Yamashit:** Conceptualization, Writing - review & editing, Supervision, Project administration.

Declaration of Competing Interest

The authors reported no declarations of interest.

Acknowledgements

This study was financially supported by the National Natural Science Foundation of China (21707020, 41425015, 41731279, 21406075), the innovation team project of Guangdong Provincial Department of Education (2017KCXTD012), and Guangdong Provincial Key R&D Programme (2019B110206002). The synchrotron radiation experiments for XAFS measurements were performed at the BL01B1 beam line in SPring-8 with the approval from JASRI (no. 2017A1063 and 2018B1185).

Appendix A. Supplementary data

Supplementary material related to this article can be found, in the online version, at doi:https://doi.org/10.1016/j.apcatb.2020.119511.

References

[1] R. Raja, V.B. Golovko, J.M. Thomas, A. Berenguer-Murcia, W.Z. Zhou, S.H. Xie, B.F.G. Johnson, Highly efficient catalysts for the hydrogenation of nitro-substituted aromatics, Chem. Commun. (2005) 2026–2028.
[2] T.C. Wang, N. Lu, J. Li, Y. Wu, Plasma-TiO_2 catalytic method for high-efficiency remediation of p-Nitrophenol contaminated soil in pulsed discharge, Environ. Sci. Technol. 45 (2011) 9301–9307.
[3] J. Yang, B. Pan, H. Li, S. Liao, D. Zhang, M. Wu, B. Xing, Degradation of p-Nitrophenol on biochars: role of persistent free radicals, Environ. Sci. Technol. 50 (2016) 694–700.
[4] S. Wunder, Y. Lu, M. Albrecht, M. Ballauff, Catalytic activity of faceted gold nanoparticles studied by a model reaction: evidence for substrate-induced surface restructuring, ACS Catal. 1 (2011) 908–916.
[5] B. Valiauga, L. Miseviciene, M.H. Rich, D.F. Ackerley, J. Sarlauskas, N. Cenas, Mechanism of two-/four-Electron reduction of nitroaromatics by oxygen-insensitive nitroreductases: the role of a non-enzymatic reduction step, Molecules 23 (2018) 1672-.
[6] K. Zhang, J.M. Suh, J.W. Choi, H.W. Jang, M. Shokouhimehr, R.S. Varma, Recent Advances in the Nanocatalyst-Assisted NaBH4 Reduction of Nitroaromatics in Water, ACS Omega 4 (2019) 483–495.
[7] H. Yu, W. Tang, K. Li, S. Zhao, H. Yin, S. Zhou, Enhanced catalytic performance for hydrogenation of substituted nitroaromatics over Ir-Based bimetallic nanocatalysts, ACS Appl. Mater. Interfaces 11 (2019) 6958–6969.
[8] G. Vile, N. Almora-Barrios, N. Lopez, J. Perez-Ramirez, Structure and reactivity of supported hybrid platinum nanoparticles for the flow hydrogenation of functionalized nitroaromatics, ACS Catal. 5 (2015) 3767–3778.
[9] M. Chatterjee, T. Ishizaka, T. Suzuki, A. Suzuki, H. Kawanami, In situ synthesized Pd nanoparticles supported on B-MCM-41: an efficient catalyst for hydrogenation of nitroaromatics in supercritical carbon dioxide, Green Chem. 14 (2012) 3415–3422.
[10] A. Furube, S. Hashimoto, Insight into plasmonic hot-electron transfer and plasmon molecular drive: new dimensions in energy conversion and nanofabrication, NPG Asia Mater. 9 (2017) e454.
[11] Y. Kuwahara, Y. Yoshimura, K. Haematsu, H. Yamashita, Mild deoxygenation of Sulfoxides over plasmonic molybdenum oxide hybrid with dramatic activity enhancement under visible light, J. Am. Chem. Soc. 140 (2018) 9203–9210.
[12] Z. Lou, P. Zhang, J. Li, X. Yang, B. Huang, B. Li, Plasmonic heterostructure TiO_2-MCs/WO_{3-x}-NWs with continuous photoelectron injection boosting hot Electron for methane generation, Adv. Funct. Mater. 29 (2019) 1808696.
[13] H. Cheng, T. Kamegawa, K. Mori, H. Yamashita, Surfactant-free nonaqueous synthesis of plasmonic molybdenum oxide nanosheets with enhanced catalytic activity for hydrogen generation from Ammonia borane under visible light, Angew. Chem. Int. Ed. 53 (2014) 2910–2914.
[14] H. Yin, Y. Kuwahara, K. Mori, M. Che, H. Yamashita, Plasmonic Ru/hydrogen molybdenum bronzes with tunable oxygen vacancies for light-driven reduction of P-Nitrophenol, J. Mater. Chem. A 7 (2019) 3783–3789.
[15] Z. Bian, T. Tachikawa, P. Zhang, M. Fujitsuka, T. Majima, Au/TiO_2 superstructure-based plasmonic photocatalysts exhibiting efficient charge separation and unprecedented activity, J. Am. Chem. Soc. 136 (2014) 458–465.
[16] S. Sarina, H. Zhu, E. Jaatinen, Q. Xiao, H. Liu, J. Jia, C. Chen, J. Zhao, Enhancing catalytic performance of palladium in gold and palladium alloy nanoparticles for organic synthesis reactions through visible light irradiation at ambient temperatures, J. Am. Chem. Soc. 135 (2013) 5793–5801.
[17] J.D. Xiao, L. Han, J. Luo, S.H. Yu, H.L. Jiang, Integration of plasmonic effects and schottky junctions into metal-organic framework composites: steering charge flow for enhanced visible-light photocatalysis, Angew. Chem. Int. Ed. 57 (2018) 1103–1107.
[18] Z. Lou, M. Zhu, X. Yang, Y. Zhang, M.-H. Whangbo, B. Li, B. Huang, Continual injection of photoinduced electrons stabilizing surface plasmon resonance of non-elemental-metal plasmonic photocatalyst Cds/WO_{3-X} for efficient hydrogen generation, Appl. Catal. B-Environ. 226 (2018) 10–15.
[19] K.K. Patra, M.K. Ghosalya, H. Bajpai, S. Raj, C.S. Gopinath, Oxidative disproportionation of MoS_2/GO to MoS_2/MoO_{3-x}/RGO : integrated and plasmonic 2D-Multifunctional nanocomposites for solar hydrogen generation from near-infrared and visible regions, J. Phys. Chem. C 123 (2019) 21685–21693.
[20] H. Jun, S. Choi, M.Y. Yang, Y.S. Nam, A ruthenium-based plasmonic hybrid photocatalyst for aqueous carbon dioxide conversion with a high reaction rate and selectivity, J. Mater. Chem. A 7 (2019) 17254–17260.
[21] S.T. Gao, W.H. Liu, N.Z. Shang, C. Feng, Q.H. Wu, Z. Wang, C. Wang, Integration of a plasmonic semiconductor with a metal-organic framework: a case of Ag/Agcl@ZIF-8 with enhanced visible light photocatalytic activity, RSC Adv. 4 (2014) 61736–61742.
[22] Q. Yang, Q. Xu, S.H. Yu, H.L. Jiang, Pd Nanocubes@ZIF-8: integration of plasmon-driven photothermal conversion with a metal-organic framework for efficient and selective catalysis, Angew. Chem. Int. Ed. 55 (2016) 3685–3689.
[23] M. Wen, K. Mori, Y. Kuwahara, H. Yamashita, Plasmonic Au@Pd nanoparticles supported on a basic metal-organic framework: synergic boosting of H2 production from formic acid, ACS Energy Lett. 2 (2017) 1–7.
[24] M. Wen, G. Li, H. Liu, J. Chen, T. An, H. Yamashita, Metal-organic framework-based nanomaterials for adsorption and photocatalytic degradation of gaseous pollutants: recent progress and challenges, Environ. Sci. Nano 6 (2019) 1006–1025.
[25] Y. Zhang, Q. Li, C. Liu, X. Shan, X. Chen, W. Dai, X. Fu, The promoted effect of a metal-organic frameworks (ZIF-8) on Au/Tio_2 for CO oxidation at room temperature both in dark and under visible light irradiation, Appl. Catal. B-Environ. 224 (2018) 283–294.
[26] Y. Isaka, Y. Kawase, Y. Kuwahara, K. Mori, H. Yamashita, Two-phase system utilizing hydrophobic metal-organic frameworks (MOFs) for photocatalytic synthesis of hydrogen peroxide, Angew. Chem. Int. Ed. 58 (2019) 5402–5406.
[27] Q. Yang, Q. Xu, H.L. Jiang, Metal-organic frameworks meet metal nanoparticles: synergistic effect for enhanced catalysis, Chem. Soc. Rev. 44 (2017) 4774–4808.
[28] M. Wen, K. Mori, Y. Kuwahara, T. An, H. Yamashita, Design of single-site photocatalysts by using metal-organic frameworks as a matrix, Chem. Asian J. (2018).
[29] J. Liu, R. Li, Y. Hu, T. Li, Z. Jia, Y. Wang, Y. Wang, X. Zhang, C. Fan, Harnessing Ag nanofilm as an electrons transfer mediator for enhanced visible light photocatalytic performance of Ag@Agcl/Ag Nanofilm/ZIF-8 photocatalyst, Appl. Catal. B-Environ. 202 (2017) 64–71.
[30] Y. Zhang, Q. Li, C. Liu, X. Shan, X. Chen, W. Dai, X. Fu, The promoted effect of a metal-organic frameworks (ZIF-8) on Au/TiO_2 for CO oxidation at room temperature both in dark and under visible light irradiation, Appl. Catal. B-Environ. 224 (2018) 283–294.
[31] M.C. Wen, Y. Kuwahara, K. Mori, D.Q. Zhang, H.X. Li, H. Yamashita, Synthesis of Ce ions doped metal-organic framework for promoting catalytic H_2 production from Ammonia borane under visible light irradiation, J. Mater. Chem. A 3 (2015) 14134–14141.